ChemPubSoc Europe

DOI: 10.1002/chem.201501793

CHEMISTRY A European Journal Full Paper

Nanostructures

Self-Assembly of Tetraphenylalanine Peptides

Enric Mayans,[a, b] Gema Ballano,[c] Jordi Casanovas,[d] Angélica Díaz,[a, b] Maria M. Pérez-Madrigal,[a, b] Francesc Estrany,[e] Jordi Puiggalí,*[a, b] Carlos Cativiela,*[c] and Carlos Alemán*[a, b]

Abstract: Three different tetraphenylalanine (FFFF) based peptides that differ at the N- and C-termini have been synthesized by using standard procedures to study their ability to form different nanoassemblies under a variety of conditions. The FFFF peptide assembles into nanotubes that show more structural imperfections at the surface than those formed by the diphenylalanine (FF) peptide under the same conditions. Periodic DFT calculations (M06L functional) were used to propose a model that consists of three FFFF molecules defining a ring through head-to-tail $NH_3^+\cdots{}^-OOC$ interactions, which in turn stack to produce deformed channels with internal diameters between 12 and 16 Å. Depending on the experimental conditions used for the peptide incubation, *N*-fluorenylmethoxycarbonyl (Fmoc) protected FFFF self-assembles into a variety of polymorphs: ultra-thin nanoplates, fibrils, and star-like submicrometric aggregates. DFT calculations indicate that Fmoc-FFFF prefers a parallel rather than an antiparallel β-sheet assembly. Finally, coexisting multiple assemblies (up to three) were observed for Fmoc-FFFF-OBzl (OBzl = benzyl ester), which incorporates aromatic protecting groups at the two peptide terminals. This unusual and noticeable feature is attributed to the fact that the assemblies obtained by combining the Fmoc and OBzl groups contained in the peptide are isoenergetic.

Introduction

Since the pioneering work of Reches and Gazit in 2003,[1] in which the formation of diphenylalanine (FF) nanotubes in aqueous solution was discovered, significant efforts have been made to develop a new generation of biomaterials based on the self-assembly of aromatic peptides. Typically, the self-assembly takes place in solution and is driven by hydrophobic forces.[2] In addition to tubular nanostructures, the most-studied FF-based polymorphs are peptide spheres composed of *tert*-butoxycarbonyl (Boc) FF[3] and peptide fibrils composed of fluorenylmethoxycarbonyl (Fmoc) FF.[4] Reviews show that efforts have been essentially focused on small FF peptides,[5] which constitute the most investigated building block for the construction of peptide self-assemblies. Amazingly, research into the self-assembly of triphenylalanine (FFF) and tetraphenylalanine (FFFF) based peptides is very scarce.

Recent studies of FFF-based peptides showed that FFF, Boc-FFF, and Fmoc-FFF can self-assemble into solid fibrillary platelike nanostructures[7] ("nanoplates"), nanospheres,[8] and hydrogels,[9] respectively. In all cases, π–π stacking interactions between aromatic rings were found to play a decisive role in the formation of the supramolecular aggregates. On the other hand, Tamamis et al.[9] and Guo et al.[10] used atomistic and coarse-grained molecular dynamics (MD) simulations, respectively, to study the assembly mechanism and the molecular basis for the structural features of FFF-based peptide nanostructures. The authors found that FFF-based peptides spontaneously assembled into solid nanospheres and nanorods with substantial antiparallel β-sheet content.

Investigations of FFFF-based peptides have focused on peptide–polymer conjugates. More specifically, Castelletto and Hamley[11] studied amphiphilic FFFF-polyethylene glycol (PEG) conjugates. Results indicated that hydrophobic association into irregular aggregates occurs at low concentration, whereas well-developed β sheets only occur at higher concentration.

[a] M. Sc. E. Mayans, Dr. A. Díaz, Dr. M. M. Pérez-Madrigal, Prof. J. Puiggalí, Prof. C. Alemán
Department of Chemical Engineering, ETSEIB
Universitat Politècnica de Catalunya
Av. Diagonal 647, 08028 Barcelona (Spain)
E-mail: jordi.puiggali@upc.edu
carlos.aleman@upc.edu

[b] M. Sc. E. Mayans, Dr. A. Díaz, Dr. M. M. Pérez-Madrigal, Prof. J. Puiggalí, Prof. C. Alemán
Center for Research in Nano-Engineering
Universitat Politècnica de Catalunya, Campus Sud, Edifici C'
C/Pasqual i Vila s/n, 08028 Barcelona (Spain)

[c] Dr. G. Ballano, Prof. C. Cativiela
Departamento de Química Orgánica
Instituto de Síntesis Química y Catálisis Homogénea-ISQCH
CSIC-Universidad de Zaragoza
C/ Pedro Cerbuna, 12, 50009 Zaragoza (Spain)
E-mail: cativiela@unizar.es

[d] Dr. J. Casanovas
Department of Chemistry, Escola Politècnica Superior
Universitat de Lleida, C/Jaume II no 69, 25001 Lleida (Spain)

[e] Dr. F. Estrany
Department of Chemical Engineering, EUETIB
Universitat Politècnica de Catalunya
Comte d'Urgell 187, 08036 Barcelona (Spain)

Supporting information for this article is available on the WWW under http://dx.doi.org/10.1002/chem.201501793.

Furthermore, drying the FFFF-PEG solutions resulted in crystallization of PEG without disruption to the local β-sheet structure defined by the peptide block. The independent organization of the two counterparts of the FFFF-PEG amphiphile was explained at the microscopic level by using atomistic MD simulations.[12] On the other hand, Tzokova et al.[13] used click chemistry to prepare poly(ethylene oxide) [PEO] conjugated to FFFF with an ethyl group at the C-terminus (FFFF-OEt). The length of PEO was found to play a crucial role in the assembly. For shorter PEO blocks, PEO-FFFF-OEt nanotubes were formed by self-assembly of anti-parallel β-sheets, stabilized by surrounding PEO chains.[1] Entanglement between adjacent nanotubes resulted in the formation of soft hydrogels. In contrast, π–π stacking interactions were prevalent for conjugates with longer PEO lengths giving rise to fibers and worm-like micelles.[13b]

Self-assembled short-peptide-based materials (including FF peptides) have potential biomedical and biotechnological applications, for example in general powerful new therapies for regenerative medicine,[14] to fabricate stable drug-delivery systems with proteolytic resistance,[15] to prepare modern nanodevices,[16] and to fabricate ultrasensitive and selective sensors for the detection of toxins.[17] Despite of the importance of this new kind of material, the self-assembly of FFFF-based peptides that are not conjugated to polymer chains remains unstudied. In this work, we synthesized three FFFF-based peptides to explore the formation of ordered self-assembled nanostructures. The results were compared with those reported for shorter FF- and FFF-analogues under similar conditions. In particular, the three peptides studied in this work were FFFF, Fmoc-FFFF, and Fmoc-FFFF-OBzl (OBzl = benzyl ester; Scheme 1). Theoretical

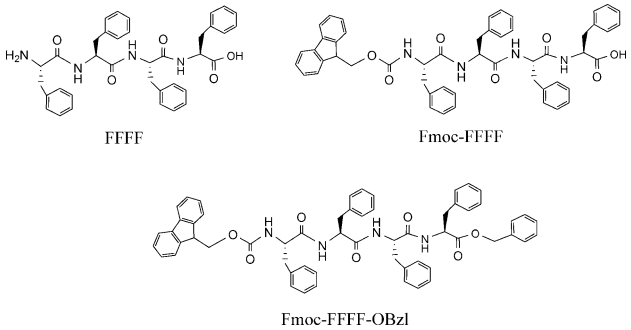

Scheme 1. Chemical structure of the FFFF-based peptides examined.

calculations for FFFF and Fmoc-FFFF aggregates were performed to get a deeper understanding of the molecular interactions involved in the self-assembly process.

Results and Discussion

Peptide synthesis

The preparation of FFFF-based peptides was carried out by following standard procedures for peptide synthesis in solution starting from the corresponding phenylalanine (F) derivative

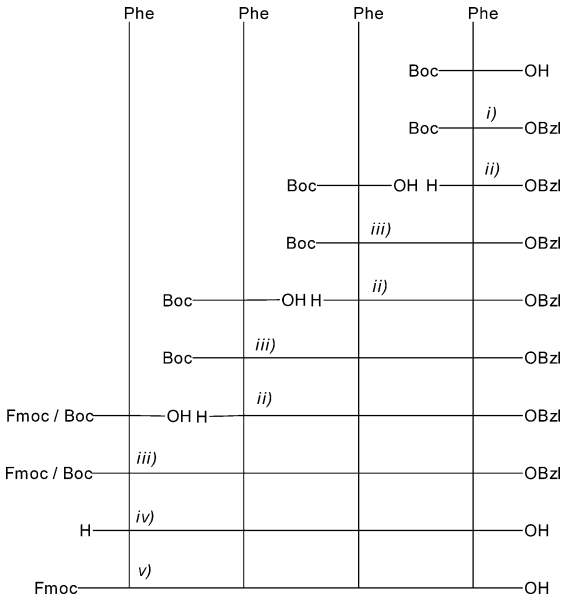

Figure 1. Scheme of the coupling reactions used to obtain FFFF, Fmoc-FFFF, and Fmoc-FFFF-OBzl. i) Boc-F-OH/benzyl bromide, THF; ii) CF_3COOH (TFA)/CH_2Cl_2 1:1; iii) 1-ethyl-3-[3-(dimethylamino)propyl]carbodiimide (EDC)/1-hydroxy-7-azabenzotriazole (HOBt), *N*-methylmorpholine (NMM; to maintain pH 8); iv) H_2/Pd, MeOH; v) FmocCl, CH_3CN.

with either a Boc or Fmoc amino protecting group. A general procedure for the coupling reactions is given in Figure 1.

FFFF nanotubes

Optical microscopy and AFM analyses of all tested conditions evidenced that FFFF self-assembles into relatively short and well-defined tubes of submicrometric thickness at 4 °C in hexafluoroisopropanol/ethanol (HFIP/EtOH) solutions with peptide concentrations ranging from 1–2 mg mL^{-1} (Figure 2a). The average diameter of these tubes (estimated by AFM) is (0.58 ± 0.12) μm, whereas the length is typically less than 100 μm. Both the length and abundance of these tubes increases noticeably when the EtOH cosolvent is replaced by water, which is reflected in the SEM images and optical micrographs displayed in Figure 2b. In this case, the thickness of the tubular structures ranges from ≈50 to ≈700 nm, and the tube was several hundreds of μm long. Interestingly, tubes obtained in HFIP/water at room temperature displayed abundant defects along the tube surface (Figure 2c), which represents a significant difference with respect to the tubes obtained at 4 °C. Furthermore, the thickness of the tubes is remarkably variable, which is reflected by the high standard deviation of the average diameter, (0.48 ± 0.37) μm. A DMF/water mixture also promotes the formation of tubular structures at 4 °C similar to those achieved in HFIP/EtOH and HFIP/water when the peptide concentration ranges from 0.1–0.5 mg mL^{-1} (Figures S1a and b in the Supporting Information). The abundance of these tubes was found to depend on the peptide concentration, with metastable tube-like assemblies being observed at very low concentrations (Figure S1c in the Supporting Information).

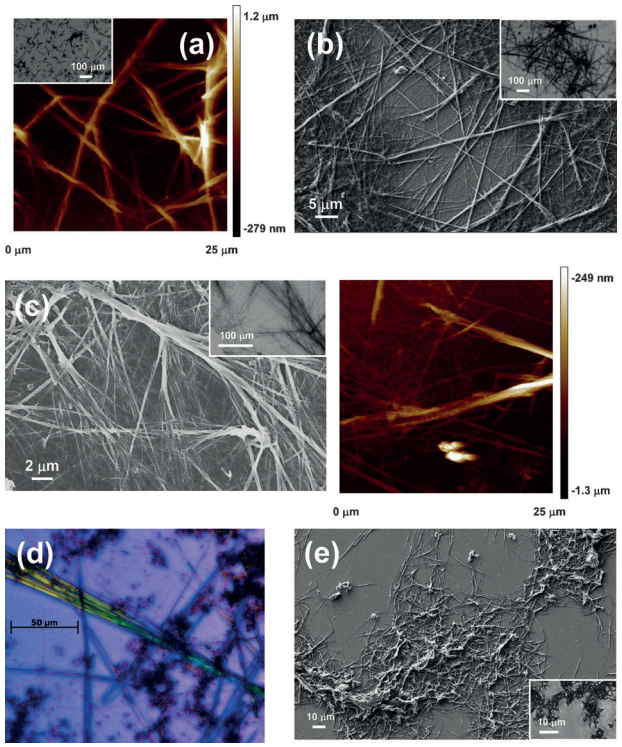

Figure 2. a) AFM image and optical micrograph (inset) of the nanotubes obtained at 4 °C for FFFF dissolved at a final concentration of 1 mg mL^{-1} in 1:4 HFIP/EtOH. b) SEM and optical microscopy (inset) images of nanotubes obtained at 4 °C for FFFF dissolved at a final concentration of 0.5 mg mL^{-1} in 1:9 HFIP/water. c) SEM, optical microscopy (inset), and AFM images of nanotubes obtained at 25 °C for FFFF dissolved at a final concentration of 0.5 mg mL^{-1} in 1:9 HFIP/water. d) Optical micrograph obtained by using cross-polarized light illumination of the fibers obtained at 4 °C for FFFF dissolved at a final concentration of 0.3 mg mL^{-1} in 3:47 DMF/water. e) SEM and optical microscopy (inset) images of tubes obtained at 4 °C for FFFF dissolved at a final concentration of 1 mg mL^{-1} in 1:4 DMF/water.

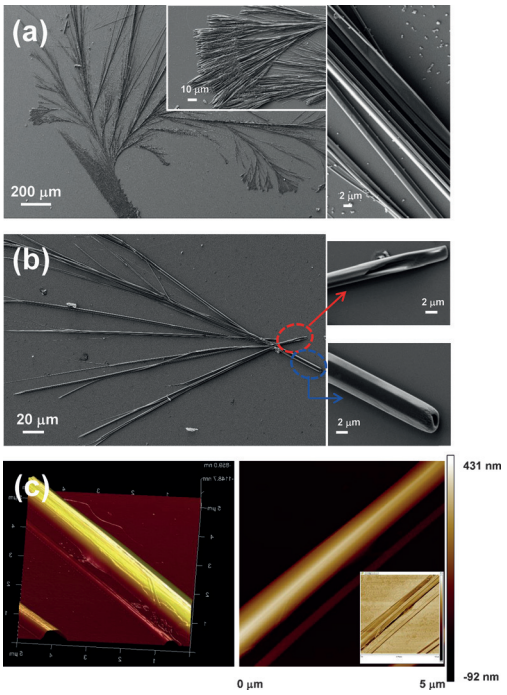

Figure 3. a) Low- and high-magnification SEM micrographs of tubes obtained at 4 °C for FF dissolved at a final concentration of 0.5 mg mL^{-1} in 1:9 HFIP/water. b) SEM micrographs and c) 3D and 2D AFM images (inset: phase image) of tubes obtained at 4 °C for FF dissolved at a final concentration of 0.3 mg mL^{-1} in 3:47 HFIP/EtOH.

The latter structures are considered to be FFFF aggregates at the early stages of the nanotube-formation process.

Microscopy using cross-polarized light illumination showed birefringence for the FFFF fibers, independent of both the solvent and the peptide concentration. This feature, which is illustrated in Figure 2d for assemblies obtained in DMF/water, indicates that the peptides retain the same orientation along the whole assembly. On the other hand, the tubes tend to aggregate in poorly defined clusters when the peptide concentration in DMF/water is $\geq$1 mg mL^{-1} (Figure 2e).

FF tubular nanostructures are typically obtained by using peptide concentrations significantly higher than those used in this work for FFFF.[1,2,5–7] To provide a comparison between the two systems, FF tubes were prepared from dilute solutions analogous to those tested for FFFF. Very well defined FF nanotubes that grew following an architecture recalling dendritic hyperbranched structures were obtained in HFIP/water at 4 °C (Figure 3a). This hyperbranched-like organization transforms into a spherulitic-nucleus-like shape when the temperature increases from 4 °C to 25 °C (Figure S2a in the Supporting Information). Despite this morphological difference, high-resolution SEM micrographs clearly indicated that the FF tubes obtained at both 25 °C and 4 °C present a smooth surface free of defects, thus they display microscopic structural differences compared with FFFF. The definition of FF tubes improves upon replacement of water by EtOH, which is evidenced in the micrographs recorded for the nanostructures derived from dilute peptide HFIP/EtOH solutions at 4 °C (Figure 3b). The root mean square (RMS) roughness and average diameter of these tubes was determined by AFM (Figure 3c) to be (40.5 $\pm$ 5.2) nm and (0.86 $\pm$ 0.09) μm, respectively. Furthermore, optical microscopy indicated that the tortuosity of the tubes increased with decreasing peptide concentration (Figure S2b in the Supporting Information). The tubes obtained at a peptide concentration of 2 mg mL^{-1} were completely straight, whereas those derived at lower concentrations showed sinuosity.

On the other hand, tube-like structures organized in dendritic branches similar to those obtained in HFIP/water were also obtained in DMF/water at 4 °C for peptide concentrations of 1–2 mg mL^{-1} (Figure S3a in the Supporting Information), whereas DMSO/water at 4 °C promoted the crystallization of FF (Figure S3b in the Supporting Information). The crystal structure of FF was reported by Görbitz[18] who found that this small peptide crystallizes with hydrogen-bonded head-to-tail chains, which form hydrophilic channels (nanotubes) embedded in a hydrophobic matrix created by the peptide side chains. Indeed, the sequence formed by two consecutive F residues was proposed to be an attractive membrane-channel model due to the substantial size of the hydrophilic channels. Interestingly, the conformation adopted by this dipeptide in

the solid state was recently identified as a minimum-energy conformation in a theoretical study.[17] It is worth noting that the crystallization conditions reported by Görbitz[18] (i.e., fast evaporation of an aqueous solution of FF (2.5 mg mL^{-1}; 3 mL) at 80 °C) were different from the conditions used in this work to obtain the monocrystals displayed in Figure S3b (see the Supporting Information). Unfortunately, FFFF monocrystals were not identified in any of the tested conditions.

To compare the molecular organization of FFFF and FF peptides in the nanotubular assemblies, DFT calculations were carried out by using the M06L functional combined with the 6-31G(d) basis set. This functional is able to account for the interactions between aromatic groups. Görbitz[18] reported that FF nanotubes are formed by six peptide units that define cyclic hexamers, which are stacked to produce narrow channels with a van der Waals diameter of ≈10 Å and a tube diameter of ≈24 Å. The oppositely charged amino- and carboxylate groups of neighboring FF molecules, which interact by forming head-to-tail $NH_3^+\cdots{}^-OOC$ hydrogen bonds, surround the inner core of the tubes. All the side chains appear to emanate from the channel core to form the hydrophobic surface. This arrangement is advantageous because it provides appropriate sites for anchoring polar molecules to the peptide matrix, which is characterized by numerous phenyl units from the FF side chains. Furthermore, Görbitz[18] found that the channel core is filled with nine crystallographic water molecules with occupancies ranging from 0.38 to 0.15.

In our approach, the crystallographic coordinates of the six FF molecules defining the hydrophilic turn were used to construct the explicit fragment of the model structure, and one-dimensional periodic boundary conditions (PBC) were applied perpendicularly to the average plane of the turn (*c*-axis) to create the three-dimensional nanotube. PBC-M06L/6-31G(d) geometry optimizations were performed considering the following starting structures:

1) the constructed nanotube (i.e., 258 explicit atoms).
2) the nanotube with six explicit water molecules, each interacting with a charged amino or carboxylate group and forming the first water layer that fills the hydrophilic core (i.e., 276 explicit atoms).
3) the structure constructed in 2) with six additional explicit water molecules defining a second water layer that interacts with the first layer (i.e., 294 explicit atoms). The position of the water molecules used in 2) and 3) were selected according to Görbitz's[18] observations for FF.

The optimized geometries reflected that, as expected, the nanotube is stable with or without water molecules filling the channel (Figure 4a). This stability was attributed to the three types of interpeptide interactions detected in the tube:

1) head-to-tail $NH_3^+\cdots{}^-OOC$ hydrogen bonds between adjacent FF molecules of the same turn; the N–H···O distances range from 1.65–1.84 Å.
2) N–H···$^-$OOC hydrogen bonds between FF molecules at different turns; the N–H···O distance (d_{H-O}) = 1.83 Å.

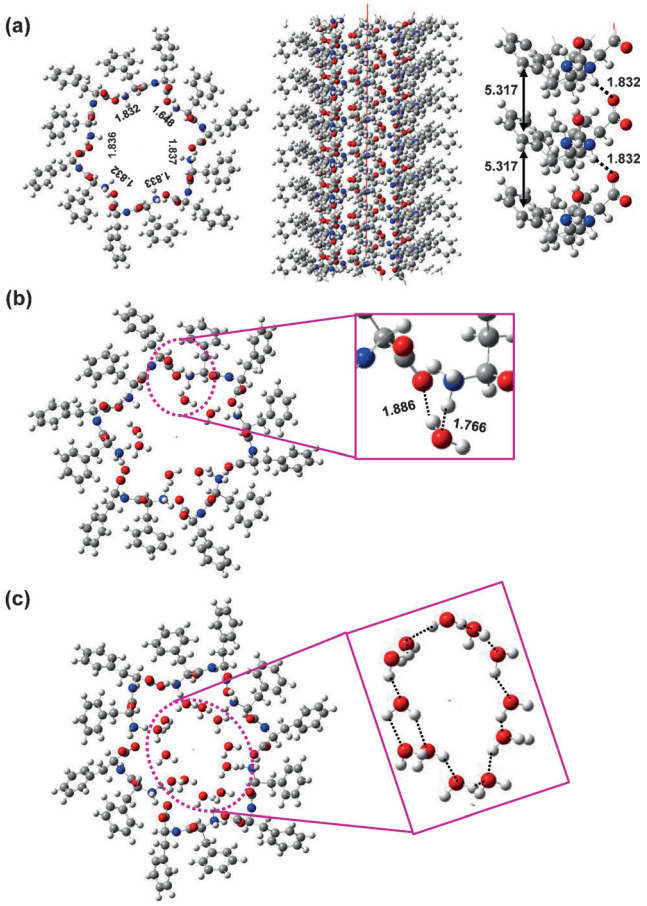

Figure 4. a) An FF nanotube derived from PBC-M06L/6-31G(d) calculations for a system with six explicit peptide molecules forming a turn. Left: top view of the six explicit FF molecules with head-to-tail $NH_3^+\cdots{}^-OOC$ hydrogen-bond distances (d_{H-O} [Å]) displayed. Middle: side view of the nanotube; the *c*-axis is represented by the red line. Right: details showing the interpeptide hydrogen bonds (d_{H-O} [Å]) and π–π stacking ($d_{\pi-\pi}$ [Å]) interactions between FF molecules located at consecutive turns. b) Top view of the FF nanotube with six explicit water molecules (first layer) filling the hydrophilic core derived from PBC-M06L/6-31G(d) calculations. Details of the hydrogen bonds formed between a water molecule and the head and the tail of different FF molecules are displayed (distances in Å). c) Top view of the FF nanotube with twelve explicit water molecules (first and second layers) filling the hydrophilic core derived from PBC-M06L/6-31G(d) calculations. Details of the hydrogen-bonded network of water molecules surrounding the hydrophilic core are displayed.

3) π–π stacking interactions between the phenyl groups of FF molecules located at different turns; the separation between the stacked rings ($d_{\pi-\pi}$) = 5.32 Å.

On the other hand, the nanotube and channel diameters are in excellent agreement with those described by Görbitz[18] (i.e., ≈24 and ≈10 Å, respectively).

The conformational parameters for the FF molecules in the three optimized structures are compared in Table S1 (see the Supporting Information) with those reported for the crystalline structure,[18] and they evidence very close agreement. The influence of water molecules on these molecular parameters is practically inexistent. Analysis of the position of the six water molecules located in the first layer after PBC-M06L/6-31G(d)

geometry optimization indicates that all the molecules, with the exception of one, interact simultaneously with two different FF molecules (Figure 4b). More specifically, each water molecule interacts with the NH_3^+ head of one peptide molecule to form an N–H···O_W–H_W hydrogen bond (O_W and H_W refers to the oxygen atom and a hydrogen atom of water, respectively) and with the $^-$OOC tail of the adjacent FF molecule at the same turn to form an O_W–H_W···$^-$OOC hydrogen bond (Figure 4b, amplified detail). This is fully consistent with the positions of the observed crystallographic water molecules,[18] which were close and connected to the charged amino and carboxylate groups. The six water molecules located in the second layer move from the starting positions to new positions located between the water molecules of the first layer (Figure 4c). As a result of this integration into the first layer, a complete hydrogen-bonded network of water molecules surrounding the hydrophilic core is obtained (Figure 4c, amplified detail).

Because of the similarity between FF and FFFF tubes, the model for FFFF was constructed considering a hexagonal disposition of three explicit peptide molecules interacting through head-to-tail NH_3^+···$^-$OOC hydrogen bonds (i.e., 249 explicit atoms). Three different conformations were found to be compatible with this turn disposition, and these were considered as starting geometries for PBC-M06L/6-31G(d) calculations. The most-stable nanotubular arrangement is represented in Figure 5a. Clearly the reduction in the number of head-to-tail interactions, which decreases from six in FF to three in FFFF, has an important effect on the nanotube morphology. Intermolecular head-to-tail interactions act as strong restraints, which limit the conformational flexibility of the molecules contained in the turn. In FFFF the number of these restraints halves and the molecular size doubles with respect to FF, therefore the conformational flexibility is significantly higher in the former. This feature is reflected in Table S1 (see the Supporting Information), which presents the average conformational parameters for the FFFF molecules. Thus, standard deviations are significantly higher than those obtained for FF.

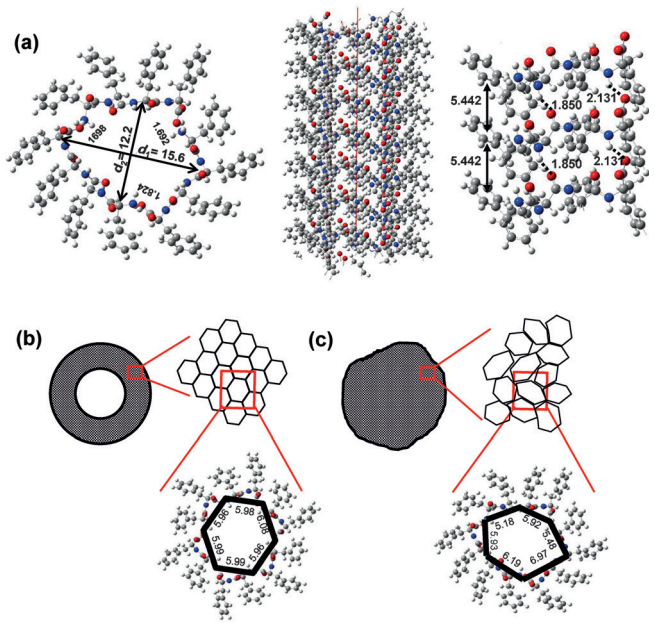

Figure 5. a) FFFF nanotube derived from PBC-M06L/6-31G(d) calculations on a system with three explicit peptide molecules forming a turn. Left: top view of the three explicit FFFF molecules with head-to-tail NH_3^+···$^-$OOC hydrogen-bonding distances (d_{H-O} [Å]) displayed. Middle: side view of the nanotube; the *c*-axis is represented by the red line. Right: Details showing interpeptide hydrogen bonds (d_{H-O} [Å]) and π–π stacking ($d_{π-π}$ [Å]) interactions between FFFF molecules located at consecutive turns. Schematic representations of the self-assembly of b) FF and c) FFFF units into tubes. FF and FFFF channels self-associate to form regular and irregular honeycomb-like arrays, respectively, which give rise to tubes.

As a result of the reduction in the number of restraints, the hexagonal symmetry observed in the FF model is lost and the shape of the FFFF tubes becomes relatively irregular with respect to that of the FF dipeptide (i.e., pseudohexagonal symmetry). This provokes a reduction in the strength of the intermolecular interactions between the FFFF molecules of consecutive turns. The d_{H-O} value associated with the N–H···$^-$OOC hydrogen bonds increases from 1.83 Å in FF to 2.13 Å in FFFF, whereas $d_{π-π}$ increases from 5.32 Å in FF to 5.44 Å in FFFF. However, an additional N–H···O=C hydrogen bond between two FFFF molecules at different turns is formed with d_{H-O} = 1.85 Å. The loss of symmetry also provokes irregularities in the empty hydrophilic core, the dimension of which cannot be determined by a single parameter (i.e., the diameter in the case of FF). Accordingly, the dimensions of the central hole in FFFF nanotubes have been defined by considering two parameters d_1 and d_2 (Figure 5a; d_1 = 15.6 Å, d_2 = 12.2 Å). It should be emphasized that the same conclusions can be reached by considering the two constructed models of higher energy (not shown), which only differ from that displayed in Figure 5 by the conformation of the peptide molecules.

The calculations presented in this section explain the morphological differences between the FF and FFFF tubes. In both cases, the narrow channels obtained by the stacking of cyclic arrays of peptide molecules self-associate to produce sheets. The coiling of such sheets generates nano- and microscale tubes for the two peptides. However, the perfect hexagonal symmetry of the FF channels, which is induced by conformational restraints provoked by regular distribution of the head-to-tail interactions, promotes perfect hexagonal packing (Figure 5b). The assembly of these sheets generates tubes that exhibit very homogeneous and regular walls without apparent surface defects (Figure 3). In contrast, the conformational flexibility of the FFFF units, which is not reduced by head-to-tail interactions, results in the formation of FFFF channels with poorly defined pseudohexagonal symmetry (Figure 5c). This provokes the generation of irregular sheets that self-assemble into tubes with irregular walls and relatively frequent surface defects (Figure 2).

Fmoc-FFFF

N-Fmoc-protected FFFF assembles into nanostructures that are completely different to the nanotubes described for FFFF and FF. More specifically, in HFIP/water Fmoc-FFFF forms well-defined ultra-thin nanoplates that aggregate in microclusters

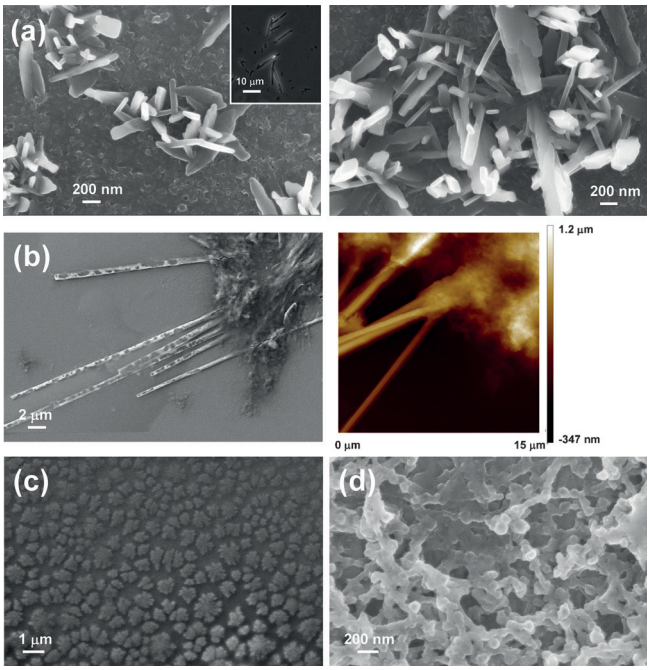

Figure 6. a) Representative SEM and optical microscopy (inset) images of nanoplates obtained at room temperature from Fmoc-FFFF dissolved at a final concentration of 0.5 mg mL^{-1} in 1:9 HFIP/water. b) SEM (left) and AFM (right) images of fibril structures obtained at 4 °C from Fmoc-FFFF dissolved at a final concentration of 0.3 mg mL^{-1} in 3:47 HFIP/EtOH. c) SEM micrograph of irregular star-like structures obtained at 4 °C from Fmoc-FFFF dissolved at a final concentration of 0.5 mg mL^{-1} in 1:9 HFIP/EtOH. (d) SEM micrograph of ill-defined nanospherical aggregates obtained at room temperature from Fmoc-FFFF dissolved at a final concentration of 1 mg mL^{-1} in 1:4 HFIP/water.

(Figure 6a). Replacement of water by EtOH as the cosolvent results in the formation of peptide fibrils at peptide concentrations <0.5 mg mL^{-1} (Figure 6b; average diameter $=(535\pm150)$ nm), whereas irregular star-like structures of submicrometric dimensions (average diameter $=(0.96\pm0.25)$ μm) appear at higher peptide concentrations (Figure 6c). Poorly defined nanospherical aggregates were obtained at Fmoc-FFFF concentrations of 1 mg mL^{-1} in HFIP/water (Figure 6d). Accordingly, the polymorphism of Fmoc-FFFF is largely influenced by the experimental incubation conditions (i.e., concentration and solvents). Polymorphism was also displayed by Fmoc-FF, which was found to self-assemble into peptide fibrils[4] similar to those displayed in Figure 6b for Fmoc-FFFF, and into hydrogels,[19] which were not identified for Fmoc-FFFF. The transformation between these two polymorphs in DMSO/water mixtures has been recently examined.[20] Thus, Fmoc-FF assembled into fibrous networks that formed gels upon addition of water. Rigid gels were obtained at high water concentrations and very low peptide concentrations (i.e., 0.01 wt%). The formation of gels under physiological conditions has been reported for Fmoc-FFF, which was produced by using an enzymatic reaction that links Fmoc-F to FF.[8] However, no other polymorph (e.g., nanoplates, nanofibrils, or submicrometric star-like aggregates) has been reported for this *N*-Fmoc-protected FFF analogue. These results indicate that the driving force responsible for the Fmoc-FFFF assemblies is different from the head-to-tail hydrogen bonds involved in the FFFF nanotubes. Indeed, previous work by several groups demonstrated that the driving force for the self-assembly of Fmoc-protected peptides is the π–π stacking of aromatic Fmoc units.[21]

The nanoplates and fibrils displayed in Figure 6a have been associated with the organization of Fmoc-FFFF molecules into β-sheet assemblies. In a previous study of FFF assemblies[6] the relationship between the nanoplates and sheet assemblies was detected by spectroscopic methods. In this work, we compared the relative stability of parallel and antiparallel Fmoc-FFFF β-sheet configurations by two different computational strategies. In the first strategy, M06L/6-31G(d) calculations were performed considering small β-sheet models with three explicit Fmoc-FFFF molecules arranged in a parallel or antiparallel fashion. The second approach is based on PBC-M06L/6-31G(d) calculations of β-sheet models constructed from two explicit Fmoc-FFFF molecules and PBC along the *c*-axis. Furthermore, four different arrangements that differ in the relative orientation of the aromatic side chains of adjacent molecules were constructed for each packing configuration. Therefore, eight structures were considered in total.

The results derived from the two strategies were fully consistent in terms of both the relative energy and stabilizing interaction patterns. The two strategies predicted that the lowest-energy β-sheet assembly corresponds to a parallel configuration. Thus, DFT calculations with explicit and periodic models indicated that the most-favored parallel and antiparallel arrangements are separated by an energy gap of 10.0 and 10.7 kcal mol^{-1}, respectively. Figures 7a and b depict the most favored parallel and antiparallel periodic models, respectively. The corresponding models derived from calculations with three explicit molecules are represented in Figure S4 (see the Supporting Information).

The intermolecular interactions found in the most-stable arrangement of each β-sheet configuration were almost identical for the explicit and periodic models. More specifically, the lowest-energy parallel arrangement (Figure 7a) is stabilized by π–π interactions involving Fmoc···Fmoc and F···F pairs, in which the aromatic rings of each pair are disposed cofacially, and by N–H···O=C hydrogen bonds (see amplified detail in Figure 7a). On the other hand, the most-favored antiparallel arrangement (Figure 7b) exhibits π–π stacking interactions involving Fmoc···F pairs, in which the aromatic rings adopt cofacial dispositions.

DFT and PBC-DFT calculations indicate that Fmoc-FFFF prefers a parallel β-sheet configuration, which is in agreement with the model proposed by Nilsson and co-workers for Fmoc-F derivatives containing fluorinated phenylalanine residues.[22] The authors proposed that the stacking of the Fmoc residues and the exposure of the C-terminus favors the parallel configuration. This model differs from that reported by Smith et al.[19a] for Fmoc-FF and by Castelletto et al.[23] for Fmoc-βAH (Fmoc-β-alanine-histidine), which both are based on antiparallel stacking. More recently, preferred parallel and antiparallel β-sheet configurations for Fmoc-GRDS and Fmoc-RGDS (G = glycine, R = arginine, D = aspartic acid, S = serine), respectively, have been proposed.[24] This led us to conclude that the β-sheet ar-

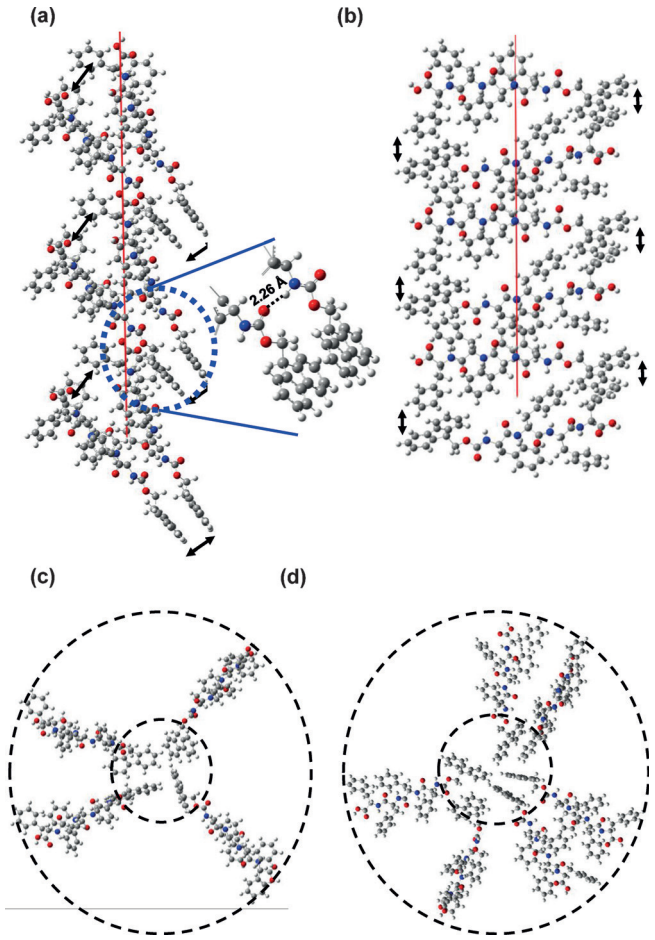

Figure 7. a) Parallel and b) antiparallel Fmoc-FFFF β-sheets derived from PBC-M06L/6-31G(d) calculations on systems with two explicit peptide molecules. The sheet axis (——) and intermolecular π–π stacking interactions (↔) are depicted. Amphiphilic lateral association of c) four and d) six explicit Fmoc-FFFF molecules. Dashed circles define the boundaries of the outer- and inner regions, which contain the polar carboxylate and the aromatic Fmoc groups, respectively.

rangement of short Fmoc peptides depends on the peptide length and sequence.

Despite the stability of the β-sheet structure, other assemblies based on π–π association of Fmoc groups can be considered for Fmoc-FFFF. Figures 7c and d show the lateral association of four (440 atoms) and six (660 atoms) explicit Fmoc-FFFF molecules, respectively, after geometry optimization at the M06L/6-31G(d) level. These amphiphilic organizations, in which the unprotected C-terminal carboxylate groups are exposed to the environment, whereas the aromatic Fmoc groups occupy the inner region, are exclusively stabilized by π–π interactions in the central core. Such stability increases with the number of molecules, which is revealed by the average binding energy experienced by each molecule (four-molecule unit = −12.3, six-molecule unit = −41.5 kcal mol^{-1}). This lateral association represents an alternative to the β-sheet organization, which may explain the existence of assemblies other than nanoplates and fibrils.

Fmoc-FFFF-OBzl

To get more insight about the role of π–π stacking interactions in the self-assembly of FFFF-based peptides, a new derivative was prepared by blocking the free carboxylate group of Fmoc-FFFF with a benzyl ester group. Fmoc-FFFF-OBzl, which has aromatic groups at both the N- and C-termini, exhibited a wide variety of assemblies depending on the experimental conditions. For example, different polymorphs were identified in HFIP/water at 4 °C depending on the peptide concentration (or on the solvent/cosolvent ratio). Ultrasmall nanoplates (≈80 and ≈35 nm length and width, respectively; Figure 8a) were obtained at very low peptide concentrations (0.05 mg mL^{-1}). In contrast, birefringent irregular agglomerates (Figure 8b) and three-dimensional clusters of triaxial ellipsoid-like nodules (Figure 8c) were formed at a peptide concentrations of 2 mg mL^{-1}

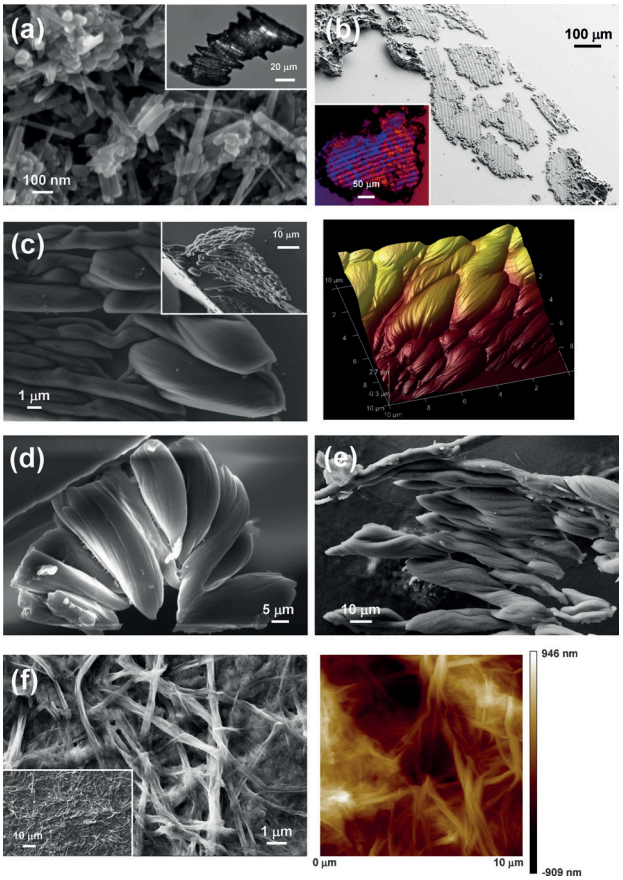

Figure 8. Representative SEM and optical microscopy (inset) images of a) nanoplates obtained at 4 °C from Fmoc-FFFF-OBzl dissolved at a final concentration of 0.05 mg mL^{-1} in 1:99 HFIP/water without sonication and b) birefringent irregular agglomerates obtained at 4 °C after sonication (35 min at 27 °C) from Fmoc-FFFF-OBzl dissolved at a final concentration of 2 mg mL^{-1} in 4:6 HFIP/water. c) Representative SEM (left) and AFM (right) images of triaxial ellipsoid-like nodules obtained at 4 °C without sonication from Fmoc-FFFF-OBzl dissolved at a final concentration of 2 mg mL^{-1} in 4:6 HFIP/water. d), e) SEM micrographs of complex organizations obtained at 4 °C from Fmoc-FFFF-OBzl dissolved at a final concentration of 4 mg mL^{-1} in 4:1 HFIP/water without sonication. f) Representative SEM and AFM micrographs of fibril entanglements obtained at room temperature from Fmoc-FFFF-OBzl dissolved at a final concentration of 0.5 mg mL^{-1} in 1:9 DMSO/water without sonication.

from sonicated and nonsonicated samples, respectively. This feature indicates that, in this case, sonication facilitates the formation of self-assembled structures. The average dimensions of the ellipsoid-like nodules (determined from the AFM images) were $a=4.2$ μm, $b=1.6$ μm and c (height) $=300$ nm (assuming $a \geq b \geq c$) (Figure 8c). These nodules were also observed for higher peptide concentrations (e.g., 4 mg mL^{-1}) when the water content is less than the HFIP content (i.e., 4:1 HFIP/water). Amazingly, these particular conditions provoked restructuring of the nodules into higher organizations, for example a feather headdress resembling a bird's tail (Figure 8d) or braided microfibers (Figure 8e). On the other hand, compact fibrillar frameworks (Figure 8f) were obtained at room temperature for peptide concentrations of 0.3–0.5 mg mL^{-1} in DMSO/water. The average dimensions of these fibrils, which form abundant entanglements (evidenced by high-resolution SEM micrographs), are 15–30 μm long and 280–420 nm thick. AFM measurements indicate that the surface roughness of the fibers is (30±5) nm, which increases to (60±8) nm in the entangled regions.

Use of HFIP as the solvent led to unusual results at 4 °C: different types of assemblies coexisted in this sample. These repetitive and reproducible observations are illustrated in Figure 9a, which displays the simultaneous presence of three very different assemblies achieved at a relatively high peptide concentration (5 mg mL^{-1}): 1) micrometric volcano-like structures that resemble microcontainers, 2) groups of ellipsoid-like nodules, and 3) very well defined tubes, similar to those obtained for FF and FFFF.

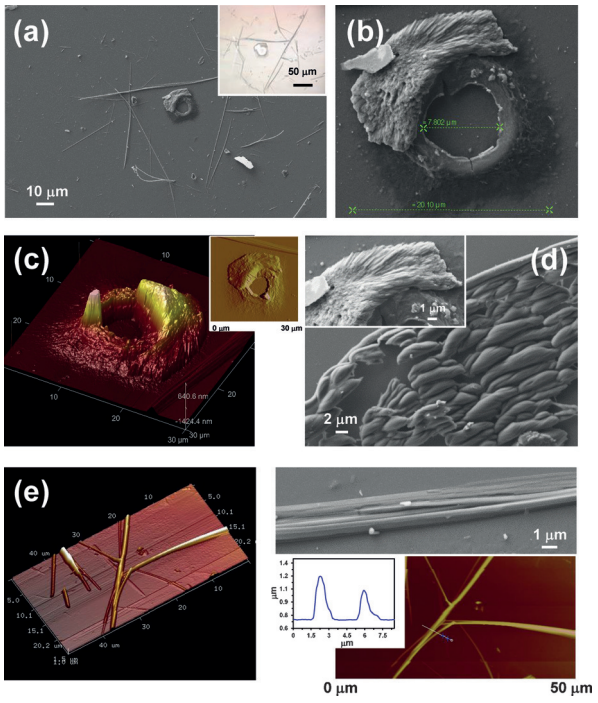

Figure 9. Assemblies obtained at 25 °C from Fmoc-FFFF-OBzl dissolved at a final concentration of 5 mg mL^{-1} in pure HFIP. a) Representative SEM and optical microscopy (inset) images showing the three different coexisting assemblies. b) SEM micrograph and c) 3D and 2D (inset) AFM height images showing the dimensions and topography, respectively, of the microcontainer (or volcano-like) assembly. d) Representative SEM micrographs of the agglomerates formed by triaxial ellipsoid-like nodules that wrap one of the slopes of the volcano in a) and b). e) Representative 3D and 2D AFM height images and SEM micrograph of the tubes. Cross-sectional profile of the zone marked in the 2D AFM image displaying the height of the tube.

The diameter of a representative volcano-like structure is ≈20 μm, and the diameter of the central hole is ≈8 μm (Figure 9b). The RMS roughness at the surface of the microcontainer sides, with heights between 1.5 and 3.0 μm, is (420±25) nm (Figure 9c. On the other hand, high-resolution SEM images (Figure 9d) indicate that the ellipsoid-like nodules, which partially wrap the sides of the microcontainer in Figure 9b, are similar to those obtained in HFIP/water at 4 °C (Figure 8c). This is corroborated by the average dimensions of the two largest axes ($a=5$ μm, $b=1.5$–2.5 μm) determined by SEM. Detailed inspection of Figure 9d suggests that these ellipsoid-like nodules are made of stacks of stretched fibers.

The thickness (≈1.9 μm) of the tubes obtained at the conditions described above was determined by SEM (Figure 9e), and the height (≈490 nm) was measured by AFM (Figure 9e). The apparent discord between the thickness and the height of the tubes is attributed to a surface-induced flattening of the assembly. This surface-induced deformity is significantly larger than that observed in cylindrical nanosized single molecular objects, for example dendronized polymers,[25] but similar to that observed for hyperbranched dendrimers[26] and tubes made of self-assembled cyclic peptides.[27]

The coexistence of up to three assemblies obtained under the above-mentioned conditions is attributed to the different intermolecular π–π stacking interactions that can be achieved by combining the multiple aromatic groups of Fmoc-FFFF-OBzl. Thus, the stabilities associated with these different interactions are probably very similar in HFIP, which permits simultaneous formation of different types of assemblies at large-enough peptide concentrations. This assumption was corroborated by the fact that samples obtained at low peptide concentrations in HFIP provided a variety of individual structures without any clear preference.

Conclusion

We synthesized three FFFF-based peptides with different flanking groups: FFFF, Fmoc-FFFF, and Fmoc-FFFF-OBzl. Unprotected FFFF forms head-to-tail $NH_3^+\cdots{}^-OOC$ hydrogen bonds, which are cannot form upon incorporation of the *N*-Fmoc and *C*-OBzl protecting groups, which promotes π–π stacking interactions.

Spontaneous assembly of the FFFF peptide results in the formation of nanotubes that resemble those achieved for FF. However, detailed microscopy studies reveal that the tubes obtained from FFFF present many surface irregularities and defects that are not present in the structures derived from FF. Theoretical DFT calculations using periodic conditions indicate that the intrinsic conformational flexibility of FFFF promotes the formation of irregular nanotubes that give surface defects upon packing. In contrast, the conformational flexibility of FF, which is intrinsically lower than that of FFFF, is restricted by the strong head-to-tail $NH_3^+\cdots{}^-OOC$ hydrogen bonds, which fa-

cilitates the formation of very regular hexagonal channels that self-associate into homogeneous tubular structures free of surface defects. Calculations also indicated that intermolecular interactions involving peptide molecules at consecutive turns of the nanotube (i.e., N–H···O hydrogen bonds and π–π stacking interactions between aromatic side chains) play a very important role in the stability of the assembly.

The variety of assemblies increases significantly for Fmoc-FFFF. Nanoplates, fibrils, star-like aggregates, and ill-defined nanospheres have all been identified for Fmoc-FFFF depending on the incubation conditions. The existence of these polymorphs suggests that π–π stacking interactions involving Fmoc groups are more versatile than hydrogen bonds in terms of molecular self-association. This is consistent with the fact that π–π interactions are considerably less specific than hydrogen bonds, which are severely restricted by the relative disposition of the N–H and C=O bonds. DFT calculations with both explicit and periodic models indicate that Fmoc-FFFF prefers a parallel rather than an antiparallel β-sheet organization. Furthermore, the ability of Fmoc aromatic groups to form π–π interactions favors the stabilization of other amphiphilic assemblies, which is consistent with the experimental observation of a variety of polymorphs.

Finally, the coexistence of up to three polymorphs in the same sample has been observed for Fmoc-FFFF-OBzl. Individual structures were detected for this peptide in HFIP/water and DMSO/water, however the most-noticeable result corresponds to the simultaneous presence of microcontainer (or volcano-like) structures, triaxial ellipsoid-like nodules, and nanotubes in samples prepared from a high concentration of peptide in HFIP. This behavior is attributed to the fact that the stability of the different combinations of intermolecular π–π stacking interactions allowed by the Fmoc and OBzl protecting groups and the phenyl side chains are similar under the experimental conditions.

Experimental Section

Materials

Boc- and Fmoc-protected amino acids were supplied by the PolyPeptide Group, *N*-[3-(dimethylamino)-propyl]-*N'*-ethylcarbodiimide was purchased from Bachem, and all other reagents for peptide synthesis were purchased from Sigma–Aldrich.

Peptide synthesis

Melting points were determined with a Gallenkamp apparatus and are uncorrected. IR spectra were recorded with a Thermo Nicolet Avatar 360 FTIR spectrophotometer; $\tilde{\nu}_{max}$ is given for the main absorption bands. ^{1}H- and ^{13}C NMR spectra were recorded with a Bruker AV-400 instrument at room temperature unless otherwise indicated; the residual solvent signal is used as an internal standard, chemical shifts (δ) are expressed in ppm, and coupling constants (J) are expressed in Hz. Optical rotations were measured with a JASCO P-1020 polarimeter. High-resolution mass spectra were obtained with a Bruker MicrOTOF-Q spectrometer.

Preparation of the initial peptide solutions

Peptide solutions (25 or 100 μL) were prepared from 5 mg mL^{-1} stock solutions in HFIP, DMSO, or DMF. Milli-Q water or EtOH were added as cosolvents to reduce the peptide concentration and enhance the assembly process. All organic solvents were purchased from Sigma–Aldrich. The peptide concentrations in the prepared solutions were 0.05–5 mg mL^{-1}. Aliquots (10 or 20 μL) were placed on microscope coverslips and kept at room temperature (25 °C) or inside a cold chamber (4 °C) until dry.

Optical microscopy

Optical morphologic observations were performed with a Zeiss Axioskop 40 microscope. Micrographs were taken with a Zeiss AxiosCam MRC5 digital camera.

Scanning electron microscopy

SEM studies were performed in a Focused Ion Beam Zeiss Neon 40 scanning electron microscope operating at 5 kV, equipped with an energy-dispersive X-ray spectroscopy system. Samples were mounted on double-sided adhesive carbon discs and sputter-coated with a thin layer of carbon to prevent sample charging problems.

Atomic force microscopy

Topographic AFM images were obtained by using either a Dimension 3100 Nanoman AFM or a Multimode instrument, both from Veeco (NanoScope IV controller) under ambient conditions in tapping mode. The RMS roughness was determined by using the statistical application of the Nanoscope software and calculates the average result considering all the values recorded in the topographic image with exception of the maximum and the minimum. AFM measurements were performed on various parts of the films, which gave reproducible images similar to those displayed in this work. Scan-window sizes were 25×25, 15×15, and 5×5 μm^2.

Theoretical calculations

DFT calculations were performed on two different types of structures: 1) those in which one-dimensional PBC were applied to an assembly previously constructed from a given number of explicit peptide molecules, and 2) those exclusively based on the assembly of explicit peptide molecules. All DFT calculations were carried out by using the Gaussian 09 computer package.[28] The geometries of the different systems investigated were fully optimized by using the M06L[29] functional, which was developed by Zhao and Truhlar to account for dispersion, combined with the 6-31G(d) basis set. PBC were used as implemented in the Gaussian 09 program (i.e., periodic systems were simply specified through a translation vector to indicate the replication direction).[30] The number of replicated cells was six in all cases, and the *k*-point mesh (NK point) in the replicated direction was set to 64, 33, and 21 for FF, FFFF, and Fmoc-FFFF, respectively. No symmetry constraints were used in the geometry optimizations. Binding energies (BEs) were corrected with the basis set superposition error (BSSE) by means of the standard counterpoise.

General procedure for the peptide coupling

1-Hydroxybenzotriazole (HOBt) (4.40 mmol) was added to a solution of the appropriately N-protected α-amino acid or peptide carboxylic acid (4.00 mmol) in CH_2Cl_2, and the solution was cooled to 0 °C

in an ice bath. *N*-[3-(dimethylamino)-propyl]-*N'*-ethylcarbodiimide hydrochloride (4.40 mmol) was added, followed by a solution of the amino component (4.40 mmol) in CH_2Cl_2 (obtained after acidic removal of the protecting group) and *N*-methylmorpholine (NMM) (4.40 mmol) or *N*-ethyldiisopropylamine (DIPEA) (4.40 mmol). The reaction mixture was stirred for 1 h at 0 °C, then at RT for 24 h at pH 8 (moistened pH paper). The reaction mixture was repeatedly washed with a 5% aqueous solution of $KHSO_4$, a 5% aqueous solution of $NaHCO_3$, and water. The organic phase was dried over $MgSO_4$ and evaporated to dryness. The peptide product was purified by flash chromatography. A description of all intermediates is provided in the Supporting Information.

FFFF: White solid; m.p. 234 °C; $[\alpha]_D^{20}$: +10.1 (c=0.43, AcOH); IR (nujol) $\tilde{\nu}$=3800–3000, 3296, 1734, 1693, 1634 cm^{-1}; HRMS (ESI): *m/z* calcd for $C_{36}H_{39}N_4O_5$: 607.2915 $[M+H]^+$; found: 607.2923. (Due to poor solubility it was impossible to record the NMR spectra in typical NMR solvents: $[D_6]$DMSO, $MeOD_4$, $CDCl_3$, CD_3CN), therefore we recorded the NMR spectra of the TFA salt.

TFA·FFFF: ^{1}H NMR (400 MHz, $[D_6]$DMSO): δ=2.72–2.88 (m, 3H), 2.91–3.12 (m, 5H), 3.90–4.00 (m, 1H), 4.46–4.53 (m, 1H), 4.56–4.65 (m, 2H), 7.14–7.32 (m, 20H), 8.31–8.76 ppm (m, 3H); ^{13}C NMR (100 MHz, $[D_6]$DMSO): δ=36.70, 37.12, 37.64, 37.74, 53.11, 53.48, 53.65, 53.86, 126.24, 126.34, 126.45, 127.09, 128.03, 128.08, 128.15, 128.22, 128.47, 129.14, 129.23, 129.56, 134.79, 137.38, 137.43, 137.46, 137.63, 168.01, 170.33, 170.65, 170.96, 172.70 ppm.

Fmoc-FFFF: White solid; m.p. 238 °C; $[\alpha]_D^{20}$: −9.6 (c=0.36, AcOH); ^{1}H NMR (400 MHz; $[D_6]$DMSO): δ=2.63–2.86 (m, 4H), 2.92–3.14 (m, 4H), 4.06–4.22 (m, 4H), 4.34–4.59 (m, 3H), 7.05–7.42 (m, 24H), 7.53 (d, J=8.8 Hz, 1H), 7.56–7.63 (m, 2H), 7.83–7.91 (m, 2H), 8.04 (d, J=8.0 Hz, 1H), 8.04 (m, 1H), 8.22 ppm (d, J=6.4 Hz, 1H); ^{13}C NMR (100 MHz, $[D_6]$DMSO): δ=36.96, 37.40, 37.62, 46.53, 53.60, 53.86, 54.15, 56.03, 65.65, 120.06, 125.24, 125.32, 126.13, 127.06, 127.61, 127.96, 128.00, 129.18, 137.61, 137.69, 138.01, 138.15, 140.63, 143.68, 143.78, 155.61, 170.56, 170.60, 171.18 ppm; IR (nujol) $\tilde{\nu}$= 3283, 1736, 1696, 1641 cm^{-1}; HRMS (ESI): *m/z* calcd for $C_{51}H_{48}N_4O_7Na$: 851.3415 $[M+Na]^+$; found: 851.3402.

Fmoc-FFFF-OBzl: White solid; m.p. 189 °C; $[\alpha]_D^{20}$: −13.2 (c=0.35, AcOH); ^{1}H NMR (400 MHz, $[D_6]$DMSO): δ=2.64–2.88 (m, 4H), 2.90–3.10 (m, 4H), 3.93–4.29 (m, 4H), 4.49–4.68 (m, 3H), 5.03–5.11 (m, 2H), 6.96–7.68 (m, 32H), 7.80–7.90 (m, 2H), 8.04 (d, J=7.9 Hz, 1H), 8.21 (d, J=7.9 Hz, 1H), 8.61 ppm (d, J=7.2 Hz, 1H); ^{13}C NMR (100 MHz, $[D_6]$DMSO): δ=36.72, 37.41, 37.67, 46.53, 53.44, 53.59, 53.72, 56.04, 65.65, 66.05, 120.02, 120.05, 121.37, 125.23, 125.31, 126.14, 126.23, 126.58, 127.05, 127.28, 127.60, 127.90, 127.96, 128.01, 128.29, 128.34, 128.92, 129.06, 129.14, 129.17, 129.24, 135.66, 136.86, 137.48, 137.51, 138.14, 140.64, 143.68, 143.76, 155.62, 170.64, 171.09, 171.19 ppm; IR (KBr): $\tilde{\nu}$=3276, 1738, 1696, 1639 cm^{-1}; HRMS (ESI): *m/z* calcd for $C_{58}H_{54}N_4O_7Na$: 941.3885 $[M+Na]^+$; found: 941.3880.

Acknowledgements

The authors thank MINECO, FEDER (MAT2012-34498, MAT2012-36205, and CTQ2013-40855-R), Generalitat de Catalunya (XRQTC), CESCA, and Gobierno de Aragón-FSE (research group E40) for support.

Keywords: beta sheet · hydrogen bonds · nanotubes · phenylalanine · pi interactions

[1] M. Reches, E. Gazit, *Science* **2003**, *300*, 625–627.
[2] M. Reches, E. Gazit, *Phys. Biol.* **2006**, *3*, S10–19.
[3] a) N. Amdursky, M. Molotskii, E. Gazit, G. Rosenman, *Appl. Phys. Lett.* **2009**, *94*, 261907; L. Adler-Abramovich, N. Kol, I. Yanai, D. Barlam, R. Z. Shneck, E. Gazit, I. Rousso, *Angew. Chem. Int. Ed.* **2010**, *49*, 9939–9942; *Angew. Chem.* **2010**, *122*, 10135–10138.
[4] N. Amdursky, E. Gazit, G. Rosenman, *Adv. Mater.* **2010**, *22*, 2311–2315.
[5] a) X. Yan, P. Zhu, J. Li, *Chem. Soc. Rev.* **2010**, *39*, 1877–1890; b) E. Gazit, *Chem. Soc. Rev.* **2007**, *36*, 1263–1269; c) G. Rosenman, P. Beker, I. Koren, M. Yevnin, B. Bank-Srour, E. Mishina, S. Semin, *J. Pept. Sci.* **2011**, *17*, 75–87; d) R. Huang, R. Su, W. Qi, J. Zhao, Z. He, *Nanotechnology* **2011**, *22*, 245609.
[6] P. Tamamis, L. Adler-Abramovich, M. Reches, K. Marshall, P. Sikorski, L. Serpell, E. Gazit, G. Archontis, *Biophys. J.* **2009**, *96*, 5020–5029.
[7] T. H. Han, T. Ok, J. Kim, D. O. Shin, H. Ihee, H.-S. Lee, S. O. Kim, *Small* **2010**, *6*, 945–951.
[8] L. Chronopoulou, S. Lorenzoni, G. Masci, M. Dentini, A. R. Togna, G. Togna, F. Bordi, C. Palocci, *Soft Matter* **2010**, *6*, 2525–2532.
[9] P. Tamamis, L. Adler-Abramovich, E. Gazit, G. Archontis, in *From Computational Biophysics to Systems Biology 2008 (CBSB08)* (Eds.: U. H. E. Hansmann, J. H. Meinke, S. Mohanty, W. Nadler, O. Zimmermann), John von Neumann Institute for Computing (Jülich), NIC Series, *Vol. 40*, pp. 393–396.
[10] C. Guo, Y. Luo, R. Zhou, G. Wei, *Nanoscale* **2014**, *6*, 2800–2811.
[11] V. Castelletto, I. W. Hamley, *Biophys. Chem.* **2009**, *141*, 169–174.
[12] D. Zanuy, I. Hamley, C. Alemán, *J. Phys. Chem. B* **2011**, *115*, 8937–8946.
[13] a) N. Tzokova, C. M. Fernyhough, P. D. Topham, N. Sandon, D. J. Adams, M. F. Butler, S. P. Armes, A. J. Ryan, *Langmuir* **2009**, *25*, 2479–2485; b) N. Tzokova, C. M. Fernyhough, M. F. Butler, S. P. Armes, A. J. Ryan, P. D. Topham, D. J. Adams, *Langmuir* **2009**, *25*, 11082–11089.
[14] a) J. B. Matson, S. I. Stupp, *Chem. Commun.* **2012**, *48*, 26–33; b) M. Nune, P. Kumaraswamy, U. Maheswari Krishnan, S. Sethuraman, *Curr. Protein Pept. Sci.* **2013**, *14*, 70–84; c) D. M. Ryan, B. L. Nilsson, *Polym. Chem.* **2012**, *3*, 18–33.
[15] a) J. J. Panda, A. Mishra, A. Basu, V. S. Chauhan, *Biomacromolecules* **2008**, *9*, 2244–2250; b) R. Silva, D. Araujo, E. Silva, R. Ando, W. Alves, *Langmuir* **2013**, *29*, 10205–10212.
[16] a) S. Cavalli, F. Albericio, A. Kros, *Chem. Soc. Rev.* **2010**, *39*, 241–263; b) A. Lakshmanan, S. Zhang, C. A. Hauser, *Trends Biotechnol.* **2012**, *30*, 155–165.
[17] a) L. Adler-Abramovich, M. Badihi-Mossberg, E. Gazit, J. Rishpon, *Small* **2010**, *6*, 825–831; b) J. H. Kim, J. Ryu, C. B. Park, *Small* **2011**, *7*, 718–722.
[18] C. H. Görbitz, *Chem. Eur. J.* **2001**, *7*, 5153–5159.
[19] a) A. M. Smith, R. J. Williams, C. Tang, P. Coppo, R. F. Collins, M. L. Turner, A. Saiani, R. V. Ulijn, *Adv. Mater.* **2008**, *20*, 37–41; b) J. Raeburn, G. Pont, L. Chen, Y. Cesbron, R. Lévy, D. J. Adams, *Soft Matter* **2012**, *8*, 1168–1174.
[20] N. A. Dudukovic, C. F. Zukoski, *Langmuir* **2014**, *30*, 4493–4500.
[21] a) Z. Yang, B. Xu, *Chem. Commun.* **2004**, 2424–2425; b) Z. Yang, G. Liang, M. Ma, Y. Gao, B. Xu, *J. Mater. Chem.* **2007**, *17*, 850–854; c) S. Toledano, R. J. Williams, V. Jayawarna, R. V. Ulijn, *J. Am. Chem. Soc.* **2006**, *128*, 1070–1071; d) V. Jayawarna, M. Ali, T. A. Jowitt, A. F. Miller, A. Saiani, J. E. Gough, R. V. Ulijn, *Adv. Mater.* **2006**, *18*, 611–614; e) R. J. Mart, R. D. Osborne, M. M. Stevens, R. V. Ulijn, *Soft Matter* **2006**, *2*, 822–835; f) A. Mahler, M. Reches, M. Rechter, S. Cohen, E. Gazit, *Adv. Mater.* **2006**, *18*, 1365–1370; g) D. J. Adams, M. F. Butler, W. J. Frith, M. Kirkland, L. Mullen, P. Sanderson, *Soft Matter* **2009**, *5*, 1856–1862.
[22] a) D. M. Ryan, T. M. Doran, B. L. Nilsson, *Chem. Commun.* **2011**, *47*, 475–477; b) D. M. Ryan, T. M. Doran, S. Anderson, B. L. Nilsson, *Langmuir* **2011**, *27*, 4029–4039.
[23] V. Castelletto, G. Cheng, B. Greenland, I. W. Hamley, P. Harris, *Langmuir* **2011**, *27*, 2980–2988.
[24] a) V. Castelletto, C. M. Moulton, G. Cheng, I. W. Hamley, M. R. Hicks, A. Rodger, D. E. López-Pérez, G. Revilla-López, C. Alemán, *Soft Matter* **2011**, *7*, 11405–11415; b) D. E. López-Pérez, G. Revilla-López, I. W. Hamley, C. Alemán, *Soft Matter* **2013**, *9*, 11021–11032.
[25] a) A. D. Schlüter, A. Halperin, M. Kröger, D. Vlassopoulos, G. Wegner, B. Zhang, *ACS Macro Lett.* **2014**, *3*, 991–998; b) O. Bertran, B. Zhang, A. D. Schlüter, M. Kröger, C. Aleman, *J. Phys. Chem. C* **2015**, *119*, 3746–3753.
[26] A. Mecke, I. Lee, J. R. Baker Jr. , M. M. B. Holl, B. G. Orr, *Eur. Phys. J. E* **2004**, *14*, 7–16.

[27] a) O. Bertran, D. Curcó, D. Zanuy, C. Alemán, *Faraday Discuss.* **2013**, *166*, 59 – 82; b) M. G. J. ten Cate, N. Severin, H. G. Börner, *Macromolecules* **2006**, *39*, 7831 – 7838.

[28] Gaussian 09, revision A.01, M. J. Frisch, G. W. Trucks, H. B. Schlegel, G. E. Scuseria, M. A. Robb, J. R. Cheeseman, G. Scalmani, V. Barone, B. Mennucci, G. A. Petersson, H. Nakatsuji, M. Caricato, X. Li, H. P. Hratchian, A. F. Izmaylov, J. Bloino, G. Zheng, J. L. Sonnenberg, M. Hada, M. Ehara, K. Toyota, R. Fukuda, J. Hasegawa, M. Ishida, T. Nakajima, Y. Honda, O. Kitao, H. Nakai, T. Vreven, J. A. Montgomery Jr., J. E. Peralta, F. Ogliaro, M. Bearpark, J. J. Heyd, E. Brothers, K. N. Kudin, V. N. Staroverov, R. Kobayashi, J. Normand, K. Raghavachari, A. Rendell, J. C. Burant, S. S. Iyengar, J. Tomasi, M. Cossi, N. Rega, J. M. Millam, M. Klene, J. E. Knox, J. B. Cross, V. Bakken, C. Adamo, J. Jaramillo, R. Gomperts, R. E. Stratmann, O. Yazyev, A. J. Austin, R. Cammi, C. Pomelli, J. W. Ochterski, R. L. Martin, K. Morokuma, V. G. Zakrzewski, G. A. Voth, P. Salvador, J. J. Dannenberg, S. Dapprich, A. D. Daniels, O. Farkas, J. B. Foresman, J. V. Ortiz, J. Cioslowski and D. J. Fox, Gaussian, Inc., Wallingford, CT, **2009**.

[29] Y. Zhao, D. G. Truhlar, *Theor. Chem. Acc.* **2008**, *120*, 215 – 241.

[30] a) K. Kudin, G. A. Scuseria, *Chem. Phys. Lett.* **1998**, *289*, 611 – 616; b) K. Kudin, G. A. Scuseria, *Phys. Rev. B* **2000**, *61*, 16440 – 16453.

Received: May 7, 2015
Published online on September 30, 2015